Xu *et al. Energy Mater* 2024;4:400076
DOI: 10.20517/energymater.2024.33

Energy Materials

Article

Open Access

Check for updates

Flame made low Pt loading catalysts supported on different metal oxides for catalytic combustion of CO and CH_4

Zuwei Xu[1,2], Ze Zhang[1,2], Fuchang Gao[1,2], Yuhan Zhu[3], Haibo Zhao[1,2,*]

[1]State Key Laboratory of Coal Combustion, School of Energy and Power Engineering, Huazhong University of Science and Technology, Wuhan 430074, Hubei, China.
[2]China-EU Institute for Clean and Renewable Energy, Huazhong University of Science and Technology, Wuhan 430074, Hubei, China.
[3]Hubei Key Laboratory of Purification and Application of Plant Anti-cancer Active Ingredients, College of Chemistry and Life Science, Hubei University of Education, Wuhan 430205, Hubei, China.

***Correspondence to:** Prof./Dr. Haibo Zhao, State Key Laboratory of Coal Combustion, School of Energy and Power Engineering, Huazhong University of Science and Technology, Wuhan 430074, Hubei, China. E-mail: hzhao@mail.hust.edu.cn

How to cite this article: Xu Z, Zhang Z, Gao F, Zhu Y, Zhao H. Flame made low Pt loading catalysts supported on different metal oxides for catalytic combustion of CO and CH_4. *Energy Mater* 2024;4:400076. https://dx.doi.org/10.20517/energymater.2024.33

Received: 20 Apr 2024 **First Decision:** 14 Jun 2024 **Revised:** 11 Jul 2024 **Accepted:** 26 Jul 2024 **Published:** 31 Jul 2024

Academic Editor: Wei Tang **Copy Editor:** Fangyuan Liu **Production Editor:** Fangyuan Liu

Abstract

Catalytic combustion is an effective approach to remove air pollutants from various emission sources. For this purpose, supported noble metal catalysts are preferred in commercial applications due to their outstanding catalytic activity for eliminating CO, hydrocarbon compounds and NOx. In this paper, we employ the flame spray pyrolysis method to prepare a series of Pt-based catalysts with four different supports (TiO_2, ZrO_2, MgO and ZnO) and variable low Pt loadings for catalytic combustion of CO and CH_4. The performance of 0.5 Pt/TiO_2 is the best in all samples, in which the T_{90} temperatures are 107 and 500 °C for 90% conversion of CO and CH_4, respectively. To examine its thermal stability, a time-on-stream test at 700 °C for 420 min is carried out, resulting in a decrease of about 5% in the final conversion of CH_4. The X-ray diffraction results show that TiO_2 support is a mixed phase with a major amount of anatase and a small amount of rutile other than a pure phase of ZrO_2, MgO and ZnO. Furthermore, X-ray photoelectron spectroscopy analysis and high-angle annular dark-field scanning transmission electron microscopy observation show that when the Pt loading is low, the Pt species exist as highly dispersed single atoms on the surface of the TiO_2 support. As the Pt loading gradually increases, the state of the Pt species transitions from single atoms to Pt clusters, resulting in a decrease in dispersion. Ultimately, the Pt can successfully

accumulate on the surface of the TiO_2 nanoparticles, providing abundant active sites for efficient catalytic combustion reactions.

Keywords: Platinum catalyst, flame spray pyrolysis, catalytic combustion, methane, carbon monoxide

INTRODUCTION

Catalytic combustion is considered to be an effective method to eliminate unburned CO and CH_4 from stationary-source and mobile-source emissions for the purpose of environmental protection[1]. Noble metals and transition metal oxides catalysts have been extensively studied to develop catalytic combustion applications[2-4]. Comparatively, supported noble metal catalysts such as platinum (Pt), palladium (Pd), rhodium (Rh) and gold (Au) have outstanding catalytic activity for CO and CH_4 oxidation, which can efficiently reduce the reaction temperature[5-7]. A commercial application is commonly used as three-way catalysts (TWCs) for CO, hydrocarbon compounds (HCs) and NOx emission control from vehicle exhausts[8]. Regarding Pt, its oxidation state is recognized as the active site for CO oxidation, whereas its metallic state is generally considered to be the active phase for CH_4 oxidation[9,10]. However, because only a small portion of the metal atoms on the surface serve as active catalytic sites, the overall efficiency, based on the total number of metal atoms, is relatively low. This is one of the reasons for the high cost of precious metal catalysts[11]. Reducing the supported state of noble metals from particles to clusters, and even down to single atoms, is an effective way to achieve maximum utilization efficiency of noble metal atoms and tunable chemical activity[12]. To better understand this important process, numerous experimental and theoretical studies have been reported about various catalytic reactions on single-atom catalysts (SACs), indicating that SACs can demonstrate excellent cost-effectiveness as well as outstanding reaction activity and selectivity in catalytic oxidation processes[13-15].

Nevertheless, the synthesis of stable SACs for high-temperature applications remains difficult because single atoms are easily mobile and tend to aggregate due to the thermodynamic driving force[16]. The aggregating phenomena dramatically reduce the amount of available active sites, resulting in a decrease or even deactivation of catalytic reactivity. Hence, it is challenging to synthesize SACs that can concurrently possess considerable durability and activity. Generally, properties of catalysts are closely related to the state of the active phase such as dispersion, valence state, and metal-support interaction[9,17]. The interaction between metal and support is believed to play a critical role in anchoring the active atoms[16]. Typical metal-support interactions include charge transfer, interface refactoring, and strong metal-support interaction (SMSI), depending on active metal and supporting matrix[18]. Therefore, the selection of appropriate supports remains a key step toward the fabrication of efficient and stable SACs. Typical catalyst supports include non-metallic oxides (SiO_2), reducible metal oxides (TiO_2, ZrO_2, CeO_2, ZnO, *etc.*), and irreducible metal oxides (Al_2O_3, MgO, *etc.*), which have been widely reported to investigate the effects of supports on the performance of SACs[19,20].

Although there are many methods to synthesize SACs, such as atomic layer deposition, impregnation, coprecipitation, and photochemical methods, these techniques usually have time-consuming preparation processes and low yields[21]. Besides conventional wet chemical methods, high-temperature synthesis techniques, such as flame spray pyrolysis (FSP), have attracted immense attention for fabricating SACs, which can be attributed to their inherent heat acclimation[22-24]. Moreover, FSP is able to handle a very wide range of precursor types and one-step synthesize nanoparticles with homogeneous morphology and narrow size distribution[25-27]. During the FSP synthesis process, the in-situ calcination-quench step provides a unique operating platform to improve the performance (activity, selectivity and stability) of SACs. Previously, our research group has used the FSP method to synthesize a series of nanomaterials for thermal

catalysis and photocatalysis, which exhibit superior activity in catalytic combustion[3,28-31], H_2 evolution[22,32], chemical looping[33], gas sensing[34], and CO_2 reduction[35]. The high-temperature flame benefits the atomization of metal species by thermal excitation and promotes the formation of stable metal-support structures. Specifically, employing the FSP method combined with precursor screening and temperature control successfully produced Pt/TiO_2 catalysts with highly dispersed surface atomic structures, achieving exceptional atomic utilization efficiency and high catalytic activity[22,31].

In this paper, we use the FSP method to synthesize a series of Pt-based catalysts with four different supports (TiO_2, ZrO_2, MgO and ZnO) and variable low Pt loadings for catalytic combustion of CO and CH_4. The catalytic activity and stability are tested and evaluated in a fixed-bed batch reactor. The morphological structure, phase composition, and surface chemical properties of samples are investigated by various physico-chemical techniques. These results demonstrate that the phase-mixed TiO_2 support shows a favorable effect on the activity and stability for CO and CH_4 oxidation. At lower loading, the Pt species are present in well-dispersed single atoms with high-valence states, while the state of the Pt species transitions from single atoms to Pt clusters as the Pt loading gradually increases. It is fascinating to note that Pt can accumulate on the surface of the TiO_2 support, which provides abundant available active sites for efficient conversion reaction.

EXPERIMENTAL

Preparation of Pt-based catalysts

Pt-based catalysts with different metal oxide supports were synthesized at a lab-scale FSP facility (Tethis NPS10, as shown in Figure 1) according to the following procedure. Firstly, support precursor solutions were prepared with titanium n-butoxide ($C_{16}H_{36}O_4Ti$, Sinopharm chemical reagent), zirconium n-propanol ($C_{12}H_{28}O_4Zr$, 70 wt% in n-propanol, Aladdin), magnesium acetate tetrahydrate ($C_4H_6O_4Mg{\cdot}4H_2O$, AR level, Aladdin), and zinc naphthenate [$C_{22}H_{14}O_4Zn$, 10% (Zn by wt.%) in mineral spirits, Alfa Aesar] as the precursors of TiO_2, ZrO_2, MgO, and ZnO, respectively. The desired amounts of each support precursor were dissolved in ethanol (for Ti, Zr, Mg) or xylene (for Zn) with a metal atom concentration of 0.3 mol/L. Then, a quantity of platinum acetylacetonate ($C_{10}H_{14}O_4Pt$, Aladdin) as a Pt source was blended in the support solution. We arranged four distinct Pt doping levels for each support, with catalyst samples denoted as rPt/Support (e.g., 0.1 Pt/TiO_2), where r represented the percent mole ratio (r mol%) of platinum to support metal element.

During the synthesis process, the precursor solution was filled into a two-fluid spray nozzle using a syringe pump; oxygen then acted as dispersion gas to atomize the precursor flow in the flame reactor. A premixed methane/oxygen pilot flame provided a hot co-flow gas to ignite the precursor spray and create a high-temperature flame, where the precursors were transformed into oxides that resulted in the formation of nanoparticles. Then, the hot flue gas was cooled to ambient temperature using air entrainment and cold sheath gas. Finally, with the assistance of a vacuum pump, the condensed and nucleated nanoparticle powder was collected using a glass microfiber filter. The detailed formulation and process parameters of catalyst preparation are shown in Supplementary Table 1.

Catalyst characterization

The crystal phases of the synthesized samples were analyzed using a powder X-ray diffractometer (Empyrean, PANalytical) with Cu Kα radiation (λ = 0.1542 nm). The specific surface areas (SSAs) were determined with a physisorption apparatus (Micromeritics ASAP-2020) employing the Brunauer-Emmett-Teller (BET) method. X-ray photoelectron spectroscopy (XPS) (ESCALAB 250Xi, Thermo Fisher) was used for catalyst surface analysis, calibrating the binding energy with the peak at 284.8 eV. Microstructural

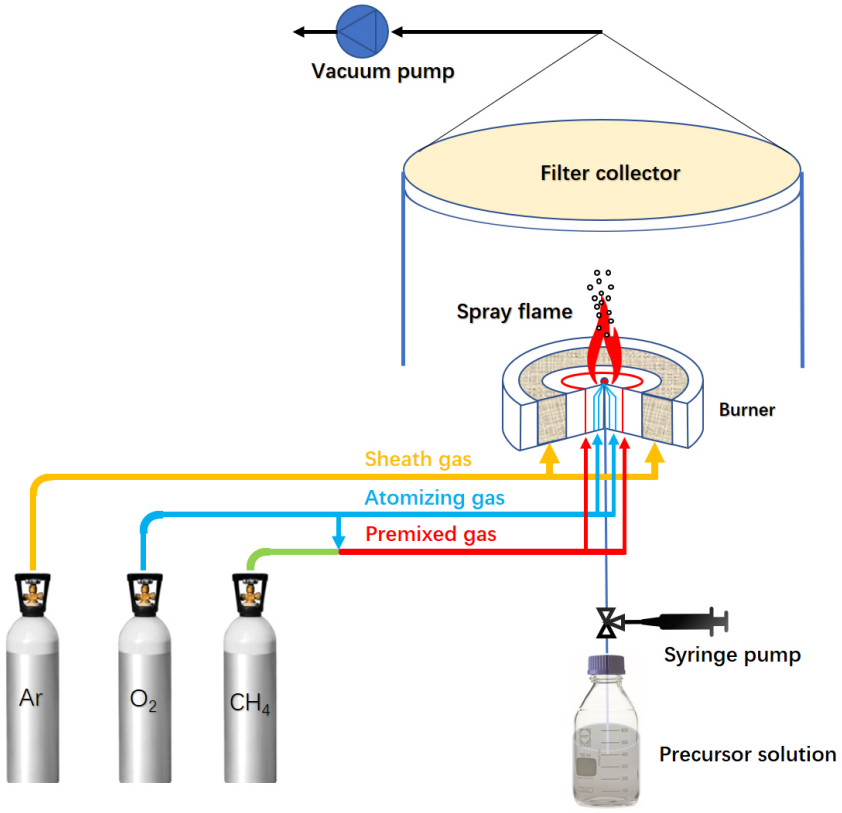

Figure 1. Schematic diagram of flame spray pyrolysis system.

characterization was carried out using a field-emission transmission electron microscope (FETEM) (Talos F200X, FEI) operating at an acceleration voltage of 200 kV. The distribution of Pt species was examined with a spherical aberration-corrected high-angle annular dark field scanning transmission electron microscope (AC-HAADF-STEM) (JEM-ARM200F, JEOL) coupled with energy dispersive spectroscopy (EDS) for elemental analysis.

The actual Pt loading in the catalyst was determined by inductively coupled plasma-optical emission spectroscopy (ICP-OES) (Agilent 5110, USA). And probing the overall Pt dispersion information on the catalyst surface by CO pulse adsorption test in a chemisorption apparatus (AutoChem1 II 2920).

The temperature-programmed reduction of H_2 (H_2-TPR) tests were performed to investigate the interaction between Pt and supports. For the experiments, 50 mg of fresh catalyst was loaded into a U-shaped quartz reactor equipped with a mass spectrometer (Hiden HPR 20). The sample was pretreated in Ar at 350 °C for 30 min to remove water and other impurities on the catalyst surface. After cooling to room temperature in high purity Ar, the TPR test started from room temperature to 900 °C at a ramp rate of 10 °C/min in 10 vol.% H_2/Ar mixture with a flow rate of 30 mL/min.

The temperature-programmed desorption of O_2 (O_2-TPD) tests were conducted in a continuous-flow reactor and the gas signal was detected by a mass spectrometer (Hiden HPR 20). First, 100 mg of catalyst was loaded into the reactor and treated under pure O_2 flow (50 mL/min) at 350 °C for 60 min. It was then cooled down to room temperature and the gas stream was switched to He for 60 min for complete removal

of the O_2 gas phase. Subsequently, the O_2 desorption experiment was carried out by starting the temperature ramp up to 900 °C at the rate of 10 °C/min.

Activity tests for catalytic combustion

Catalytic combustion performance tests were conducted in a fixed-bed batch reactor, as shown in Supplementary Figure 1. The system consisted of a gas feeding unit, a quartz tube furnace equipped with a temperature controller, and a gas detection unit. The gas feeding unit was used to regulate the gas flow of fuel gas CO or CH_4, as well as O_2 and Ar. During the reaction, the gas flows from the top down to ensure that the reaction is complete without blowing up the catalyst. The gas composition of the outlet after filtration and condensation was analyzed using an online mass spectrometer (Hiden HPR 20). Prior to the reaction, 100 mg of fresh catalyst was placed onto quartz wool in the middle of the reactor tube. The reactor was sealed and introduced with a 5 vol.% O_2/Ar mixture to remove air and adsorbed impurities at the flow rate of 100 mL/min under a ramp-up rate of 10 °C/min. After reaching 200 °C, the reactor was purged with Ar while cooling down to room temperature.

The catalytic activity for CO was evaluated using the gaseous mixture made of 2 vol.% CO, 5 vol.% O_2, and balance gas Ar at a weight hourly space velocity (WHSV) of 60,000 mL/(g_{cat}·h). The reaction was performed at temperatures of 50-300 °C and the catalyst was left on stream at each temperature for 3 min. In the CH_4 catalytic combustion experiment, a higher proportion of O_2 was set in the gas mixture to enable complete oxidation of CH_4. The gas mixture consisting of 2 vol.% CH_4, 12 vol.% O_2, and balance gas Ar was fed at a WHSV of 60,000 mL/(g_{cat}·h). The reaction temperature was set in the range of 200-700 °C. Moreover, a long-cycle test for CH_4 catalytic combustion was held at 700 °C for 420 min to examine the thermal stability of catalysts. Moisture is an important influencing factor that needs to be considered for practical applications. In order to explore the effect of water vapor on the activation properties of the catalyst, an experimental investigation was carried out by reacting the catalyst at 700 °C for 240 min under 2 vol.% CH_4, 12 vol.% O_2, 10 vol.% water vapor and balance gas Ar, fed at a WHSV of 60,000 mL/(g_{cat}·h).

The conversion X of CO or CH_4 is calculated using the gas signal from the mass spectrometer by

$$X_{CO\ /\ CH_4} = \frac{[C]_{inlet} - [C]_{outlet}}{[C]_{inlet}} \times 100\%$$

where $[C]_{inlet}$ represents the inlet concentration of CO or CH_4, and $[C]_{outlet}$ indicates the outlet concentration of CO or CH_4, respectively.

The turnover frequency (TOF) of the catalyst was calculated to analyze its reactivity by

$$TOF_{Pt} = \frac{Q \times X \times M_{Pt}}{22.4 \times m_c \times p \times D}$$

where Q represents the flowrate of CO in L/s, and X stands for the conversion of CO, M_{Pt} signifies the molar mass of Pt in g/mol, 22.4 is the molar volume of standard gas in L/mol, m_c denotes the mass of the catalyst in g, p indicates the mass fraction of Pt in the catalyst, and D corresponds to the dispersion of Pt on the catalyst surface.

RESULTS AND DISCUSSION

Catalytic combustion performance

The catalytic activity of samples is evaluated by the characteristic temperature T_{90} that indicates the temperature required for 90% conversion of CO, and the WHSV for this condition is 60,000 mL/(g_{cat}·h). Figure 2 shows the test results of CO catalytic combustion over Pt catalysts with four different supports. T_{90} of all samples progressively decreases by raising the Pt loading from 0.025 to 0.5mol%, in which Pt/TiO_2 samples show the most dramatic drop from approximately 200 to 107 °C. It can be seen that the CO catalytic combustion activity of the other three samples is lower than that of Pt/TiO_2. For Pt/ZrO_2 catalysts, there is almost no difference in activity at low Pt loadings (0.025% and 0.05%), and the activity rose significantly when the loading increased from 0.05% to 0.5%, with the lowest T_{90} of 185 °C. Pt/ZnO samples demonstrate poor CO conversion activity, in which all of the effective conversion temperatures are over 200 °C, and 0.5 Pt/ZnO has comparable activity with 0.025Pt/TiO_2 for catalytic combustion of CO.

From the above catalytic combustion behaviors, as prepared Pt/TiO_2 samples have the best activity for CO complete conversion at lower temperatures. Thus, Pt/TiO_2 samples are selected for further tests in CH_4 catalytic combustion. As shown in Figure 3, the T_{90} temperatures for CH_4 catalytic combustion of Pt/TiO_2 samples reduce to about 500 °C with the increase of Pt content from 0.025 to 0.5 mol%. The 0.5 Pt/TiO_2 sample reaches complete combustion at about 600 °C.

In view of the characteristic that a precious metal catalyst is easy to deactivate at high temperatures, a time-on-stream test of CH_4 conversion over the 0.5 Pt/TiO_2 catalyst at a high temperature of 700 °C was conducted to examine its high-temperature stability. As shown in Figure 4A, the CH_4 conversion only slightly decreases after 420 min continuous test, about 5%. It is evidently found that 0.5 Pt/TiO_2 has good catalytic activity and stability at high temperatures. Water content is an important factor to consider in practical applications, so we investigated the influence of water vapor on catalyst activity by introducing water vapor into the system. Experimental results, as shown in Figure 4B, indicate that prior to the introduction of water vapor, the oxygen carrier exhibited stable and effective reaction activity, maintaining methane conversion rates around 96%. Upon introduction of water vapor, there was a slight decrease in catalyst activity, with methane conversion rates maintained around 92%, representing a 4% decline. This loss in catalyst activity is likely attributed to competitive adsorption of water molecules on active sites. Upon removal of water vapor again, the catalyst activity returned to its pre-introduction levels, with a negligible irreversible activity loss of less than 1%. The experiments demonstrate that our oxygen carrier exhibits good water resistance and durability against water vapor.

Catalyst characterization and analysis

A representative fresh sample (0.5% Pt loading) of each different support catalyst was selected for XRD analysis. Meanwhile, a corresponding raw support sample without Pt was used as a reference, which was synthesized by FSP under the same conditions. As shown in Supplementary Figure 2, The XRD patterns of the various catalysts reveal their phase composition and crystal structure. No diffraction peaks for Pt or Pt oxides were detected, likely due to the highly dispersed state and low content of Pt. Additionally, the TiO_2 support is present as a mixed phase, with a minor amount of rutile (crystal face [110]) and a predominant amount of anatase (crystal face [101]), and the anatase content of 0.5 Pt/TiO_2 sample (ca. 82%) is lower than that of the TiO_2 sample (ca. 89%). It suggests that Pt species can promote the phase transition from anatase to rutile in the FSP process. The other three catalyst supports are all pure phase, including cubic ZrO_2, cubic MgO, and hexagonal ZnO, respectively.

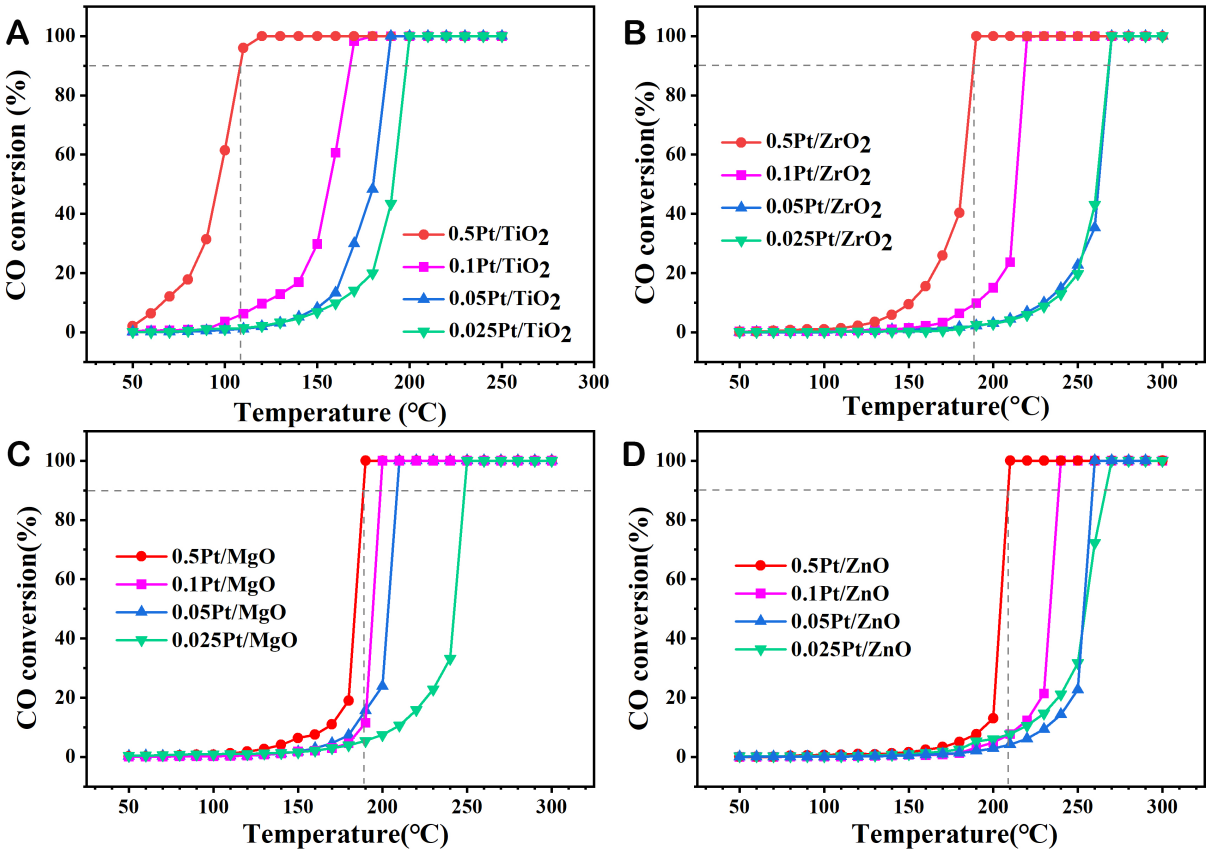

Figure 2. CO catalytic combustion test curves of (A) Pt/TiO_2, (B) Pt/ZrO_2, (C) Pt/MgO, and (D) Pt/ZnO.

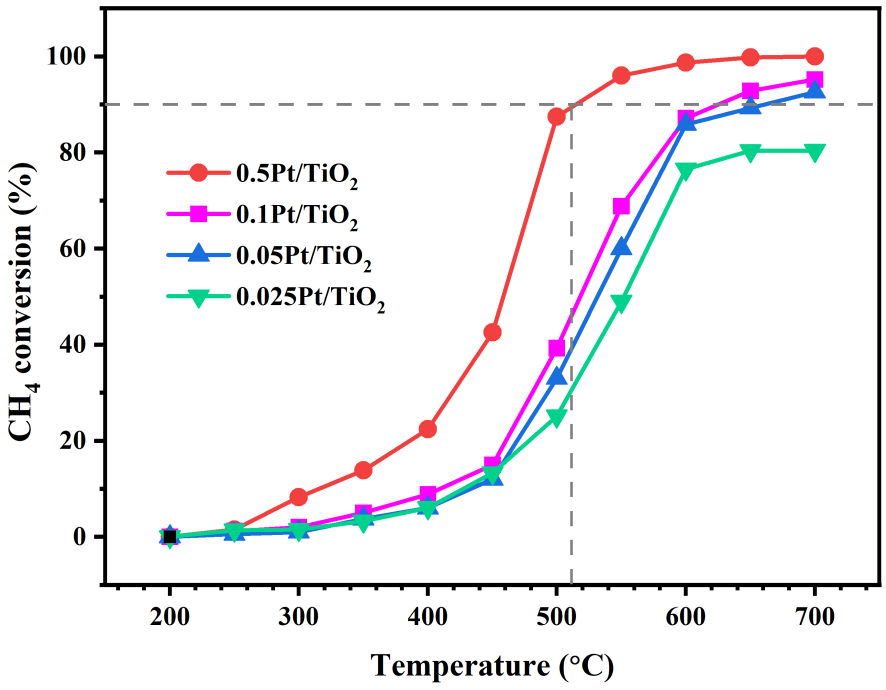

Figure 3. CH_4 catalytic combustion curves over Pt/TiO_2 catalysts.

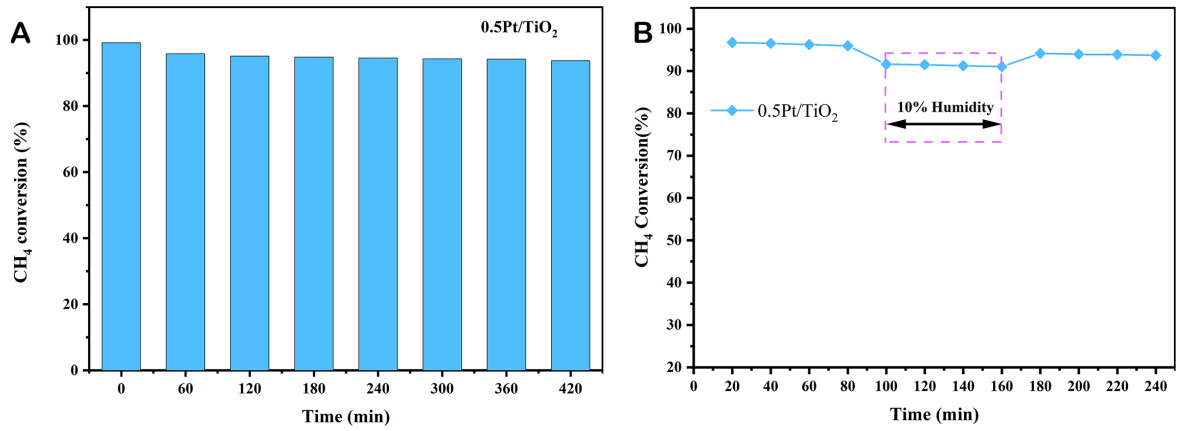

Figure 4. CH_4 conversion time-on-stream test (A) over 0.5 Pt/TiO_2 catalysts and time-on-stream test (B) in the presence of 10% water vapor with 0.5 Pt/TiO_2 at 700 °C.

XPS was used to analyze the chemical states of Pt species on support surfaces. The high-resolution Pt 4f XPS spectra of four representative samples are processed by split-peak fitting, as shown in Supplementary Figure 3. The Pt 4f XPS spectra have relatively large noise due to the low Pt loadings, which have been found to be similar in other studies of Pt catalysts. The Pt in each sample exists in three chemical states: Pt^{4+}, Pt^{2+}, and Pt^0, with most of the Pt species present in the high-valence state Pt^{4+}, while a minority in the zero-valence state Pt^0. The presence of Pt^0 is mainly due to the formation of metal Pt clusters during the synthesis process, while the high-valence state Pt can be identified as highly dispersed Pt single atoms due to the strong metal-carrier interaction (SMSI) between Pt and supports[36]. The valence state of Pt that we mention here is the valence state embodied due to the formation of coordination between Pt and O. Pt single atoms may occupy different substitution or epitaxial growth sites on the TiO_2 support, leading to Pt existing in various coordination states. However, Pt itself remains in the form of single atoms within the oxygen carrier, rather than as a compound. The different coordination states of Pt significantly influence catalytic activity; typically, Pt diffuses deeper into the lattice of the support, resulting in lower coordination states and catalytic activity[37]. Therefore, by adjusting the coordination environment of SACs, we can significantly enhance their catalytic performance. The oxygen carriers prepared in this study are in their optimal coordination state, exhibiting a +4 oxidation state, which maximizes Pt catalytic activity.

We tested the actual Pt content in the various catalysts by ICP-OES, the surface Pt contents and the proportions of Pt with different valence states by XPS. The results, as presented in Table 1, indicate that the Pt content in the different catalysts prepared reached the values designed in our preparation process. Moreover, the surface Pt content was calculated according to the XPS spectra. For each sample, it is higher than the design loading value, especially with the 0.5 Pt/TiO_2 sample, where the excess is more significant. This indicates that Pt primarily accumulates on the surface of the TiO_2 support, and the TiO_2 support surface can adsorb more Pt, which is conducive to the formation of more catalytic active sites. This also supports that 0.5 Pt/TiO_2 catalysts have the best performance in the above catalytic tests.

To further study the interaction between Pt species and TiO_2, XPS spectra of Pt/TiO_2 samples with different Pt loadings were analyzed. Figure 5A shows that the O 1s profiles can be divided into two peaks representing lattice oxygen and adsorbed oxygen. The first peak with a binding energy between 529.8 and 530.0 eV indicates lattice oxygen, and the second peak with a binding energy in 531.3-537.1 eV belongs to adsorbed oxygen that mainly involves O, O^-, or O^{2-} surface oxygen species and usually serves as active

Table 1. Pt Loading measured by ICP-OES and XPS

Catalyst	Pt/Ti (mol%)			Pt^0/Pt (mol%)
	Designed	Measured (ICP-OES)	Surface content (XPS)	
0.5 Pt/TiO_2	0.5	0.459	2.70	15.69
0.5 Pt/ZrO_2	0.5	0.481	1.90	13.69
0.5 Pt/MgO	0.5	0.453	0.87	17.57
0.5 Pt/ZnO	0.5	0.466	0.89	19.43

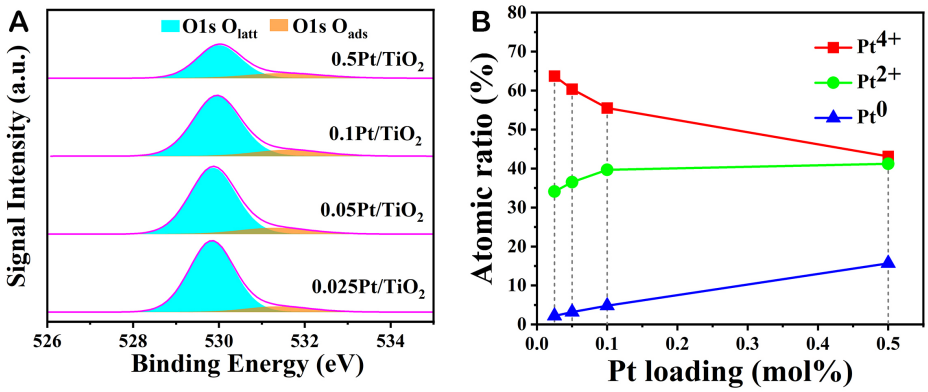

Figure 5. XPS spectra of Pt/TiO_2 samples with various Pt loadings: (A) O 1s profiles; (B) atomic ratio of Pt^0, Pt^{2+} and Pt^{4+}.

reactants in catalytic combustion[19]. Since surface adsorbed oxygen species are easily formed around oxygen vacancies, the number of surface adsorbed oxygen can reflect the number of oxygen vacancies. The proportion of adsorbed oxygen to surface oxygen (O_{ads}/O) is listed in Table 2, which increases gradually with the Pt loading. In Figure 5B, it can be seen that with rising Pt content, the concentrations of Pt^0 and Pt^{2+} in the low oxidation states gradually increase, while the concentration of Pt^{4+} in the high oxidation state decreases gradually. Especially for single-atom Pt dispersed on a TiO_2 surface, it is more favorable to form a high oxidation state.

H_2-TPR was used to compare the reduction performance of 0.5% Pt-based catalysts with different supports. As shown in Figure 6, both the hydrogen consumption peaks of Pt/TiO_2 and Pt/ZrO_2 are below 350 °C, but the hydrogen consumption of Pt/TiO_2 (0.308 mmol/g_{cat}) is significantly higher than that of Pt/ZrO_2 (0.043 mmol/g_{cat}), indicating that Pt/TiO_2 has better oxidizing properties and can provide more active oxygen for the reaction. Additionally, although the hydrogen consumption of Pt/MgO (0.387 mmol/g_{cat}) and Pt/ZnO (0.379 mmol/g_{cat}) is slightly higher than that of Pt/TiO_2, their hydrogen consumption peaks are above 350 °C, which suggests that Pt/TiO_2 has a catalytic advantage in terms of reaction temperature. In particular, the two hydrogen consumption peaks of Pt/ZnO below 400 °C correspond to the reduction of oxidized Pt and reactive oxygen species, while the larger peak width above 400 °C is the superposition of the reduction processes of reactive oxygen species and lattice oxygen of ZnO[24]. Furthermore, the hydrogen consumption peak at 250 °C in the H_2-TPR curve of 0.5 Pt/ZrO_2 is caused by surface active oxygen adsorbed on the catalyst surface, while the second hydrogen consumption peak corresponds to the reaction and release of lattice oxygen.

The H_2-TPR profiles of Pt/TiO_2 samples with various Pt loadings are shown in Figure 7. As the Pt loading increases, the reaction temperature of the Pt/TiO_2 catalyst gradually decreases. The 0.5 Pt/TiO_2 sample

Table 2. XPS analysis results of Pt/TiO_2 catalysts

Catalyst	O 1s binding energy (eV)		O_{ads}/O (mol%)	Pt^0/Pt (mol%)
	O_{latt}	O_{ads}		
0.025 Pt/TiO_2	529.83	531.39	10.23	2.63
0.05 Pt/TiO_2	529.86	531.31	12.80	3.17
0.1 Pt/TiO_2	529.95	531.62	13.34	4.81
0.5 Pt/TiO_2	530.00	531.52	21.13	15.69

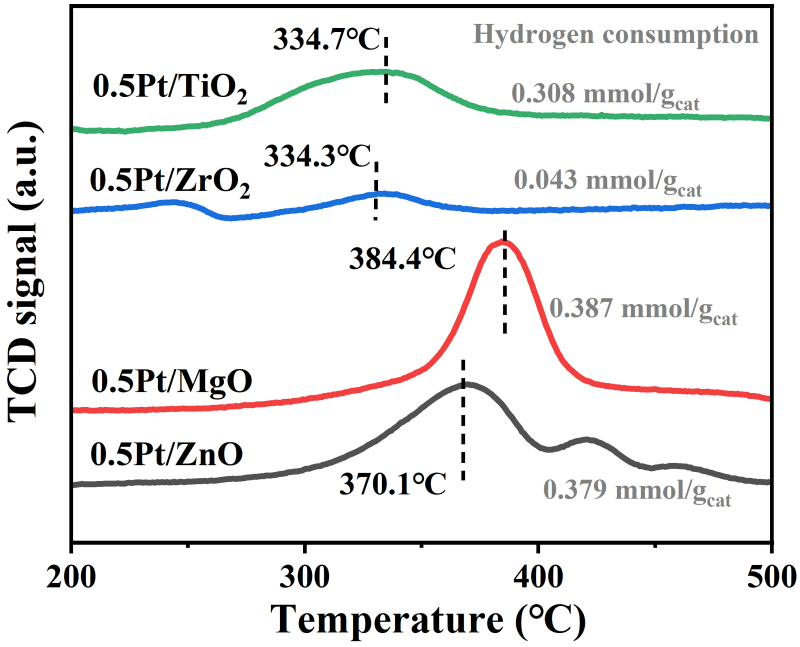

Figure 6. H_2-TPR curves of 0.5 Pt/TiO_2, 0.5 Pt/ZrO_2, 0.5 Pt/ZnO, 0.5 Pt/MgO.

shows the highest hydrogen consumption peak intensity and area, with a hydrogen consumption of up to 0.31 mmol/g_{cat}, which is almost five times that of the other three samples. This indicates that the increased Pt content enhances the interaction between Pt and TiO_2, providing more active sites and promoting the release of lattice oxygen from TiO_2. In all the samples, there is a high reduction peak with most hydrogen consumption in the range of 300~450 °C, which is attributed to the reduction of oxidized Pt species. The peaks with large width and low intensity above 400 °C correspond to the reduction of reactive oxygen species interacting with Pt and TiO_2. There is also a small peak at 0.1 Pt/TiO_2 and 0.5 Pt/TiO_2 between 100 and 200 °C, owing to the reduction of Pt in the oxidation state having weak interaction with TiO_2. The H_2-TPR results show that the interaction between Pt and TiO_2 effectively improves the oxidation capability of the catalyst, and the Ti-O bond around the supported Pt species is activated. As mentioned above, XPS results show that the 0.5 Pt/TiO_2 sample has a higher surface adsorption oxygen content, namely more oxygen vacancies, which is conducive to the migration of surface adsorbed species.

The O_2-TPD results of Pt/TiO_2 catalysts are shown in [Figure 8]. There are two desorption peaks for 0.5 Pt/TiO_2 samples at 600~700 °C and 800~900 °C, corresponding to surface lattice oxygen and bulk phase lattice oxygen, respectively. For the lower loadings of three samples, only one peak is found at 800 °C. Since surface

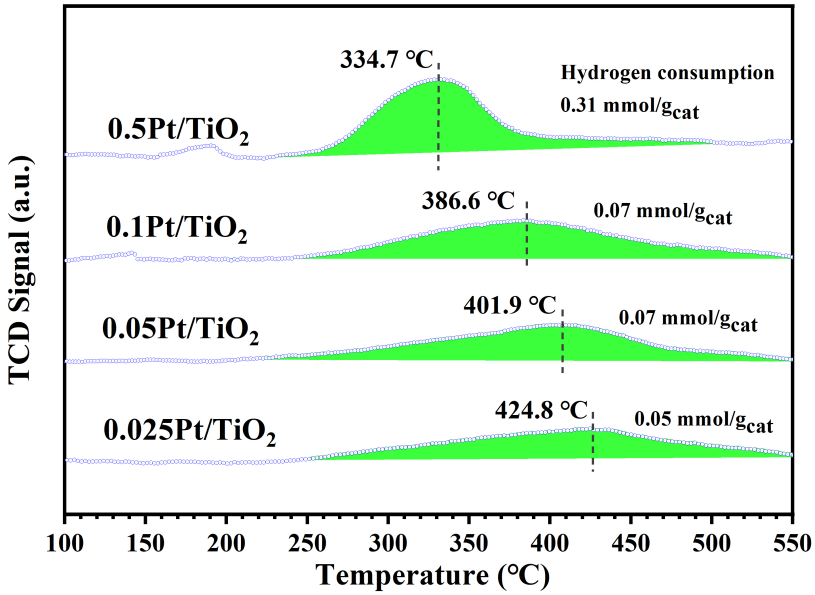

Figure 7. H_2-TPR curves of Pt/TiO_2 samples with different Pt loadings.

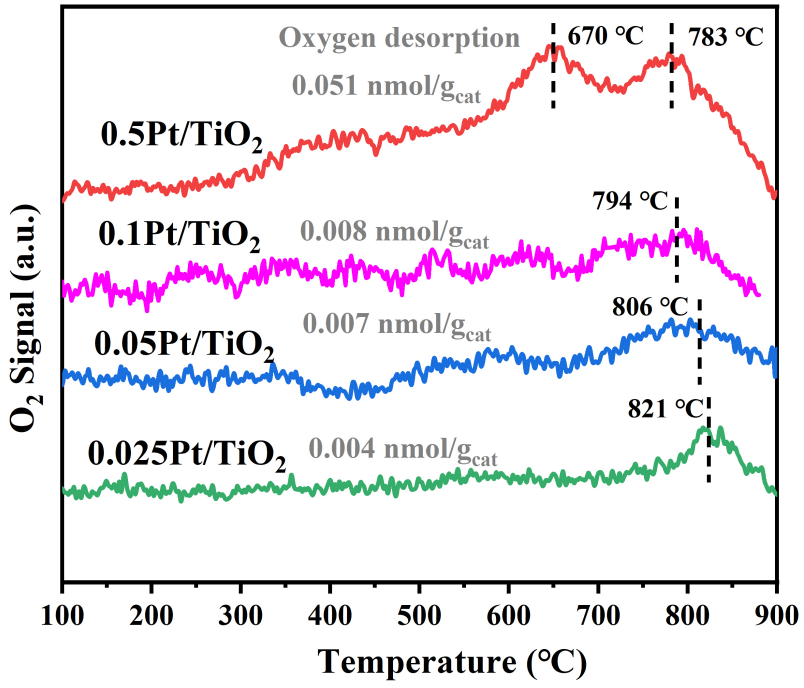

Figure 8. O_2-TPD curves of different Pt loading catalysts.

lattice oxygen is easier to release than bulk lattice oxygen, this peak corresponds to the desorption of the former. As the Pt content grows, the temperature corresponding to the oxygen desorption peak of the

samples gradually decreases. This indicates that the increase in Pt content facilitates the release of lattice oxygen from TiO_2. Additionally, with the boost in Pt content, the oxygen desorption amount of the four samples gradually rises, with the 0.5 Pt/TiO_2 sample having the highest oxygen desorption amount, reaching 0.051 nmol/g_{cat}. This shows that the increase in Pt content not only promotes the release of lattice oxygen but also aids in the conversion of oxygen into lattice oxygen. The catalytic combustion of CH_4 generally follows the M-K mechanism, where the lattice oxygen species of the catalyst are involved in the reaction[15].

Nitrogen adsorption and desorption isotherms of Pt/TiO_2 catalysts with distinct Pt contents, along with 0.5 Pt/ZrO_2, 0.5 Pt/MgO, 0.5 Pt/ZnO catalysts, are shown in Supplementary Figure 4. The curves of four Pt/TiO_2 samples have similar characteristics. When the relative pressure P/P_0 increases above 0.8, the adsorption curve of nitrogen is separated from the adsorption curve under the same relative pressure P/P_0, and the hysteresis loop appears. The hysteresis loops are H^1 type, indicating that Pt/TiO_2 samples have relatively narrow pore sizes and the characteristics of uniform spherical particle aggregates[38]. In addition, the SSA is also calculated by the BET method based on the data. The results show that the SSA of Pt/ZrO_2 is the lowest at only 56 m^2/g, while that of Pt/ZnO is a little higher as it can reach 115 m^2/g. The SSA of Pt/TiO_2, with varying Pt contents, is higher than that of Pt/ZrO_2 and Pt/ZnO in the range of 120~170 m^2/g, and the SSA of Pt/MgO is the largest, reaching up to 275 m^2/g. We found that the SSA of 0.5 Pt/MgO significantly exceeds that of other samples. Assuming the powder particles are rigid spheres, the relationship between the SSA (m^2/g) and the average particle size D (nm) is given by SSA = 6/(D*ρ), where ρ is the density of the material (g/m^3). Using this formula, we calculated the particle sizes of the 0.5 Pt/TiO_2, 0.5 Pt/ZrO_2, 0.5 Pt/MgO, and 0.5 Pt/ZnO catalysts, resulting in particle sizes of 9.6, 15.4, 14.5, and 12.5nm, respectively. The small differences in their particle sizes indicate that the SSA measurements of the catalysts are reliable. Typically, a larger catalyst surface area implies more active sites and higher catalytic activity. However, the increase in catalyst surface activity with the surface area occurs only when the active components are uniformly distributed. The experiments revealed that the catalytic activity of Pt/MgO is relatively low, which might be due to poor dispersion of Pt on MgO[39]. In contrast, Pt/TiO_2 exhibits both a large SSA and high Pt dispersion, resulting in excellent catalytic activity.

For the microstructure observation of representative samples 0.1 Pt/TiO_2 and 0.5 Pt/TiO_2, FETEM was utilized. AC-HAADF-STEM with sub-angstrom resolution was employed to analyze Pt species state. In the case of the 0.1 Pt/TiO_2 catalyst, high-resolution transmission electron microscopy (HRTEM) images [Figure 9A] revealed particles predominantly comprising anatase and rutile phases, with 10 nm diameters that are consistent with SSA analysis (BET equivalent diameter of 8.4 nm). Brightly contrasted individual Pt atoms were observed on the surface of TiO_2 support [Figure 9B], and energy-dispersive X-ray spectroscopy (EDS) confirmed the presence of Pt, Ti, and O [Figure 9C]. Moreover, HRTEM images for the 0.5 Pt/TiO_2 catalyst [Figure 9D] are similar to 0.1 Pt/TiO_2 (BET equivalent diameter of 9.6 nm). Notably, on the TiO_2 surfaces, both individual platinum atoms and platinum nanocrystals were present [Figure 9E and F]. These microstructural characterizations illustrate that with increasing Pt content, Pt transitions from single atoms to clusters. The transmission electron microscopy (TEM) analysis of 0.1 Pt/TiO_2 and 0.5 Pt/TiO_2 catalysts provided insights into Pt dispersion and state at active sites on the catalyst's microsurface. However, to assess the overall Pt dispersion across the catalyst surface, we conducted CO pulse adsorption tests. The results showed that the Pt dispersion on the surface of the 0.1 Pt/TiO_2 catalyst was 79.68%, while on the 0.5 Pt/TiO_2 catalyst, it was 39.54%. This decrease in dispersion with increased Pt content suggests that higher Pt loadings tend to form Pt clusters, leading to reduced dispersion, consistent with the observations from TEM regarding the presence of Pt on the catalyst surface.

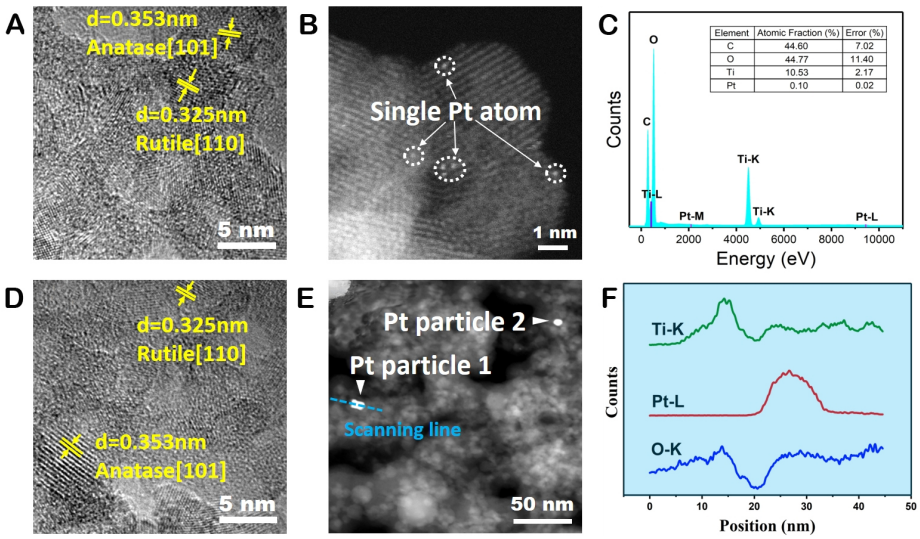

Figure 9. Microstructure characterization of 0.1 Pt/TiO_2 (A-C) and 0.5 Pt/TiO_2 (D-F): FETEM (A and D); AC-HAADF-STEM (B and E); EDS element profiles (C and F).

To more objectively evaluate the performance of our catalyst, we compared it with the performance of catalyst samples from other similar studies. The results are summarized in Figure 10; we have compared the reaction temperature and activity differences of the Pt/TiO_2 catalyst prepared by the impregnation method[40], the Pt/Al_2O_3 catalyst prepared by the incipient wetness impregnation method[41], and the Pt/TiO_2 catalyst synthesized by the FSP method in this study. As shown in Figure 10A, our Pt/TiO_2-FSP catalyst exhibits the highest CO reaction performance at low temperatures. The CO reaction performance of the Pt/TiO_2-Coimpregnation catalyst is relatively close to our catalyst. However, from Figure 10B, it is evident that the TOF of our Pt/TiO_2-FSP catalyst is significantly higher than that of the Pt/TiO_2-Coimpregnation catalyst, with the difference increasing with temperature. This can be attributed to the differences in particle size and morphology caused by the distinct preparation methods. Our FSP-synthesized catalyst consists of nano-sized particles with Pt in a single-atom state attached to the catalyst surface, whereas the co-impregnation method results in micron-sized particles with Pt present in both single-atom and Pt cluster forms, leading to differences in active site reactivity. The Pt/Al_2O_3 catalyst shows much lower CO conversion rates and CO reaction activity at low temperatures compared to both Pt/TiO_2 catalysts.

As shown in Figure 11, a schematic diagram qualitatively describes the possible reaction patterns of CO and CH_4 over two typical Pt/TiO_2 catalysts, respectively. Both CO and CH_4 react through the Mars-van Krevelen (MvK) mechanism, with the difference being that the activation center for the CO reaction is single-atom Pt, while for CH_4, it is Pt clusters. The specific reaction process does not differ and generally proceeds in two steps: first, CH_4 adsorbs onto the active Pt species on the catalyst surface, where the lattice oxygen from within the catalyst diffuses to the surface and reacts with CH_4 to produce CO_2 and H_2O, thus forming surface oxygen vacancies. Then, oxygen from the reaction atmosphere adsorbs and dissociates, generating surface oxygen, which subsequently migrates to the oxygen vacancies, replenishing them and producing lattice oxygen, completing the entire reaction cycle. Additionally, as the Pt content in the oxygen carrier increases, the Pt dispersion on the surface gradually decreases, with single Pt atoms aggregating into Pt clusters, leading to a decline in the activity of Pt adsorption sites.

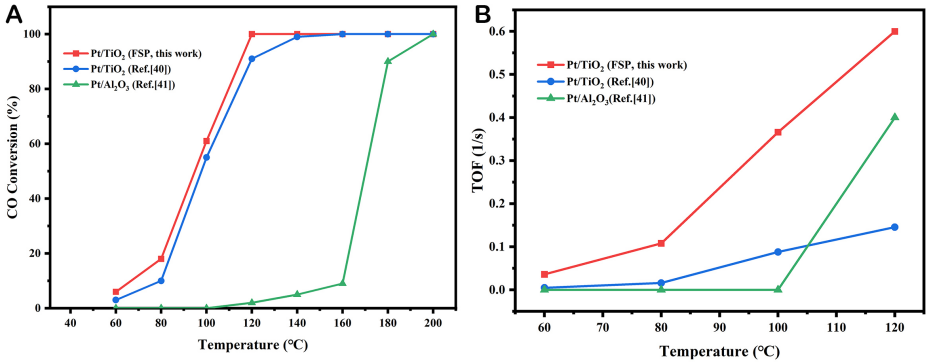

Figure 10. Comparison of (A) reaction performance and (B) reaction TOF of different Pt-doped catalysts with the Pt/TiO_2 catalyst of this study. Where Pt/TiO_2 catalysts were synthesized in the Ref.[40] using the impregnation method (test condition: 0.5% CO, 2.55% O_2, using Ar as balance, WHSV = 60,000 $mLg^{-1}h^{-1}$, 0.1wt%Pt). Pt/Al_2O_3 catalysts were synthesized in the Ref.[41] using the incipient wet impregnation method (test condition: 1% CO, 5% O_2, using Ar as balance, WHSV = 200,000 $mLg^{-1}h^{-1}$, 0.1wt%Pt).

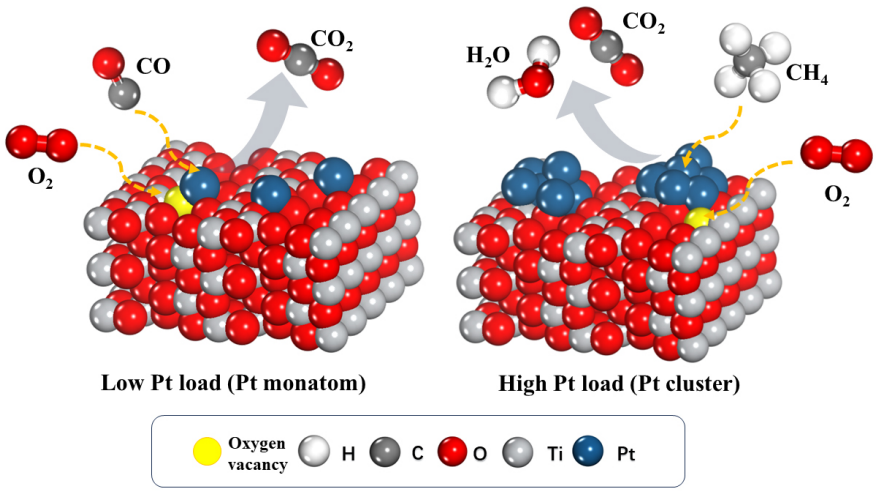

Figure 11. Schematic diagram of reaction patterns of CO and CH_4 over Pt/TiO_2.

CONCLUSIONS

A series of Pt-based catalysts are synthesized by the FSP method for catalytic combustion of CO and CH_4, which involves four different supports (TiO_2, ZrO_2, MgO and ZnO) and variable low Pt loadings (0.025%-0.5%). According to catalytic activity and stability tests, the performance of 0.5 Pt/TiO_2 is the best in all samples, in which the T_{90} temperatures are 107 and 500 °C for 90% conversion of CO and CH_4, respectively. The final conversion of CH_4 decreases by about 5% after the time-on-stream test at 700 °C for 420 min. Compared with the other three supports, TiO_2 support is a mixed phase with a major amount of anatase and a small amount of rutile other than a pure phase of ZrO_2, MgO and ZnO. The Pt/TiO_2 samples have very high SSA in the range of 120~170 m^2/g. Additionally, Pt species can promote the phase transition from anatase to rutile in the FSP process. Pt element has three chemical states: Pt^{4+}, Pt^{2+}, and Pt^0. Most of the Pt species are present in the high-valence state Pt^{4+}, whereas the zero-valence state Pt^0 is the least common. The presence of Pt^0 is mainly due to the formation of Pt clusters, while the oxidation states Pt can be identified as highly dispersed Pt single atoms. At lower loading, the Pt species are present in well-dispersed single atoms with oxidation states, and Pt transitions from single atoms to clusters as the Pt loading

increases. The synergistic effect between Pt and TiO_2 effectively enhances the catalyst's activity, and the Ti-O bond around the supported Pt species is activated. It is fascinating to note that the Pt species can be enriched on the surface of TiO_2 nanoparticles, which provides abundant available active sites for efficient conversion reaction.

DECLARATIONS

Authors' contributions

Designing research, writing the paper: Xu Z
Material characterization, formal analysis: Zhang Z
Performing research: Gao F
Data visualization: Zhu Y
Review, supervision, funding acquisition: Zhao H

Availability of data and materials

Not applicable.

Financial support and sponsorship

This work was supported by the National Natural Science Foundation of China (52376111 and 51920105009), the Hubei Province Key Research and Development Program (2022BCA087), the Natural Science Foundation of Hubei Province (2021CFB251), and the Scientific Research Project of Hubei Provincial Department of Education (Q20213002). We also thank the Analytical and Testing Center of HUST for XRD, XPS and FETEM characterization of catalysts.

Conflicts of interest

All authors declared that there are no conflicts of interest.

Ethical approval and consent to participate

Not applicable.

Consent for publication

Not applicable.

REFERENCES

1. Chen X, Xu Z, Yang F, Zhao H. Flame spray pyrolysis synthesized CuO-TiO_2 nanoparticles for catalytic combustion of lean CO. *Pro Combust Inst* 2019;37:5499-506. DOI
2. Chua YG, Gunasooriya GKK, Saeys M, Seebauer EG. Controlling the CO oxidation rate over Pt/TiO_2 catalysts by defect engineering of the TiO_2 support. *J Catal* 2014;311:306-13. DOI
3. Ding S, Chen H, Mekasuwandumrong O, et al. High-temperature flame spray pyrolysis induced stabilization of Pt single-atom catalysts. *Appl Catal B Environ* 2021;281:119471. DOI
4. Fan J, Chen Y, Jiang X, et al. A simple and effective method to synthesize Pt/CeO_2 three-way catalysts with high activity and hydrothermal stability. *J Environ Chem Eng* 2020;8:104236. DOI
5. Feng X, Jiang L, Li D, et al. Progress and key challenges in catalytic combustion of lean methane. *J Energy Chem* 2022;75:173-215. DOI
6. Fujiwara K, Pratsinis SE. Single Pd atoms on TiO_2 dominate photocatalytic NOx removal. *Appl Catal B Environ* 2018;226:127-34. DOI
7. Gong X, Song P, Han C, Xiao Y, Mei X, Xu W. Heterogeneous single-atom catalysts for energy process: recent progress, applications and challenges. *Energy Mater* 2023;3:300016. DOI
8. Gao F, Xu Z, Zhao H. Flame spray pyrolysis made Pt/TiO_2 photocatalysts with ultralow platinum loading and high hydrogen

production activity. *Pro Combust Inst* 2021;38:6503-11. DOI
9. Gong XQ, Selloni A, Dulub O, Jacobson P, Diebold U. Small Au and Pt clusters at the anatase TiO_2(101) surface: behavior at terraces, steps, and surface oxygen vacancies. *J Am Chem Soc* 2008;130:370-81. DOI PubMed
10. González-prior J, López-fonseca R, Gutiérrez-Ortiz J, de Rivas B. Catalytic removal of chlorinated compounds over ordered mesoporous cobalt oxides synthesised by hard-templating. *Appl Catal B Environ* 2018;222:9-17. DOI
11. He L, Fan Y, Bellettre J, Yue J, Luo L. A review on catalytic methane combustion at low temperatures: catalysts, mechanisms, reaction conditions and reactor designs. *Renew Sustain Energy Rev* 2020;119:109589. DOI
12. Huang C, Shan W, Lian Z, Zhang Y, He H. Recent advances in three-way catalysts of natural gas vehicles. *Catal Sci Technol* 2020;10:6407-19. DOI
13. Huang G, Niu Q, Zhang J, et al. Platinum single-atoms anchored covalent triazine framework for efficient photoreduction of CO_2 to CH_4. *Chem Eng J* 2022;427:131018. DOI
14. Jin J, Li C, Tsang C, Xu B, Liang C. Catalytic combustion of methane over Pt-Ce oxides under scarce oxygen condition. *Ind Eng Chem Res* 2016;55:2293-301. DOI
15. Li P, Chen X, Ma L, Bhat A, Li Y, Schwank JW. Effect of Ce and La dopants in Co_3O_4 nanorods on the catalytic activity of CO and C_3H_6 oxidation. *Catal Sci Technol* 2019;9:1165-77. DOI
16. Li S, Ren Y, Biswas P, Tse SD. Flame aerosol synthesis of nanostructured materials and functional devices: processing, modeling, and diagnostics. *Prog Energy Combust Sci* 2016;55:1-59. DOI
17. Lou Y, Liu J. CO Oxidation on metal oxide supported single pt atoms: the role of the support. *Ind Eng Chem Res* 2017;56:6916-25. DOI
18. Lu Y, Duan L, Sun Z, Chen J. Flame spray pyrolysis synthesized CuO-CeO_2 composite for catalytic combustion of C_3H_6. *Pro Combust Inst* 2021;38:6513-20. DOI
19. Chen Z, Xu Z, Zhao H. Flame spray pyrolysis synthesis and H_2S sensing properties of CuO-doped SnO_2 nanoparticles. *Pro Combust Inst* 2021;38:6743-51. DOI
20. Meng L, Zhao H. Low-temperature complete removal of toluene over highly active nanoparticles CuO-TiO_2 synthesized via flame spray pyrolysis. *Appl Catal B Environ* 2020;264:118427. DOI
21. Niu F, Li S, Zong Y, Yao Q. Catalytic behavior of flame-made Pd/TiO_2 nanoparticles in methane oxidation at low temperatures. *J Phys Chem C* 2014;118:19165-71. DOI
22. Qiao B, Wang A, Yang X, et al. Single-atom catalysis of CO oxidation using Pt_1/FeO_x. *Nat Chem* 2011;3:634-41. DOI
23. Schulz C, Li S. Virtual special issue of recent advances in gas-phase synthesis of functional materials for energy. *Energy Fuels* 2021;35:6341-3. DOI
24. Sun H, Tang R, Huang J. Considering single-atom catalysts as photocatalysts from synthesis to application. *iScience* 2022;25:104232. DOI PubMed PMC
25. Sun H, Zhang P, Wang J, et al. Understanding the suppressive role of catalytically active Pt-TiO_2 interfacial sites of supported metal catalysts towards complete oxidation of toluene. *J Mater Chem A* 2022;10:25633-43. DOI
26. Tang Z, Zhang T, Luo D, Wang Y, Hu Z, Yang RT. Catalytic combustion of methane: from mechanism and materials properties to catalytic performance. *ACS Catal* 2022;12:13457-74. DOI
27. Vikrant K, Weon S, Kim K, Sillanpää M. Platinized titanium dioxide (Pt/TiO_2) as a multi-functional catalyst for thermocatalysis, photocatalysis, and photothermal catalysis for removing air pollutants. *Appl Mater Today* 2021;23:100993. DOI
28. Wang A, Li J, Zhang T. Heterogeneous single-atom catalysis. *Nat Rev Chem* 2018;2:65-81. DOI
29. Wang Y, Zhang X, Cheng C, Yang Z. TiC supported single-atom platinum catalyst for CO oxidation: a density functional theory study. *Appl Surface Sci* 2018;453:159-65. DOI
30. Xiong Z, Xu Z, Li Y, et al. Incorporating highly dispersed and stable Cu^+ into TiO_2 lattice for enhanced photocatalytic CO_2 reduction with water. *Appl Surface Sci* 2020;507:145095. DOI
31. Yang F, Liu M, Chen X, Xu Z, Zhao H. Simultaneous control over lattice doping and nanocluster modification of a hybrid CuO_x/TiO_2 photocatalyst during flame synthesis for enhancing hydrogen evolution. *Solar RRL* 2018;2:1800215. DOI
32. Yang XF, Wang A, Qiao B, Li J, Liu J, Zhang T. Single-atom catalysts: a new frontier in heterogeneous catalysis. *ACC Chem Res* 2013;46:1740-8. DOI
33. Yao Y, Huang Z, Xie P, et al. High temperature shockwave stabilized single atoms. *Nat Nanotechnol* 2019;14:851-7. DOI
34. Yuan X, Meng L, Xu Z, Zheng C, Zhao H. CuO quantum dots supported by $SrTiO_3$ perovskite using the flame spray pyrolysis method: enhanced activity and excellent thermal resistance for catalytic combustion of CO and CH_4. *Environ Sci Technol* 2021;55:14080-6. DOI
35. Yuan X, Qing M, Meng L, Zhao H. One-step synthesis of nanostructured Cu-Mn/TiO_2 via flame spray pyrolysis: application to catalytic combustion of CO and CH_4. *Energy Fuels* 2020;34:14447-57. DOI
36. Yuan X, Zheng C, Xu Z, et al. The synergic removal mechanism for photothermocatalytic toluene over single-atom Pt/TiO_2 catalysts via flame spray pyrolysis. *Pro Combust Inst* 2023;39:5637-45. DOI
37. Tan W, Xie S, Le D, et al. Fine-tuned local coordination environment of Pt single atoms on ceria controls catalytic reactivity. *Nat Commun* 2022;13:7070. DOI PubMed PMC
38. Zhang L, Cheng X, Zhang G, Qiu W, He H, Chen G. High active platinum clusters on titanium dioxide supports toward carbon monoxide oxidation. *Appl Catal B Environ* 2020;266:118629. DOI

39. Tanabe T, Nagai Y, Dohmae K, Sobukawa H, Shinjoh H. Sintering and redispersion behavior of Pt on Pt/MgO. *J Catal* 2008;257:117-24. DOI
40. Einaga H, Urahama N, Tou A, Teraoka Y. CO oxidation over TiO_2-supported Pt-Fe catalysts prepared by coimpregnation methods. *Catal Lett* 2014;144:1653-60. DOI
41. Tan W, Xie S, Zhang X, et al. Fine-tuning of Pt dispersion on Al_2O_3 and understanding the nature of active Pt sites for efficient CO and NH_3 oxidation reactions. *ACS Appl Mater Interfaces* 2024;16:454-66. DOI